ACS Energy LETTERS

http://pubs.acs.org/journal/aelccp

LETTER

Electrochemical Window of the Li-Ion Solid Electrolyte $Li_7La_3Zr_2O_{12}$

Travis Thompson,[†] Seungho Yu,[†] Logan Williams,[‡] Robert D. Schmidt,[†] Regina Garcia-Mendez,[‡] Jeff Wolfenstine,[§] Jan L. Allen,[§] Emmanouil Kioupakis,[‡] Donald J. Siegel,[*,†,‡] and Jeff Sakamoto[*,†,‡]

[†]Department of Mechanical Engineering and [‡]Department of Materials Science & Engineering, University of Michigan, 2350 Hayward Avenue, Ann Arbor, Michigan 48109, United States

[§]Army Research Laboratory, RDRL-SED-C, 2800 Powder Mill Road, Adelphi, Maryland 20783, United States

Supporting Information

ABSTRACT: The recent discovery of fast ion-conducting solid electrolytes could enable solid-state and other advanced battery chemistries with higher energy densities and enhanced safety. In addition to high ionic conductivity, a viable electrolyte should also exhibit an electrochemical window that is wide enough to suppress undesirable electronic transport (i.e., self-discharge and/or short circuiting) arising from charge injection or extraction from the electrodes. Here, direct current chronoamperometry, alternating current electrochemical impedance spectroscopy, and optical absorption band gap measurements are combined with first-principles calculations to systematically characterize the electrochemical window of the promising superionic conductor $Li_7La_3Zr_2O_{12}$ (LLZO). Negligible electronic current was measured within LLZO for a wide range of voltages relevant for high-voltage cathodes. This auspicious behavior is consistent with both the large band gap (~6 eV) predicted for LLZO and the absolute positions of its band edges. These features imply that a wide electrochemical window is an intrinsic property of LLZO, facilitating its use in next-generation batteries.

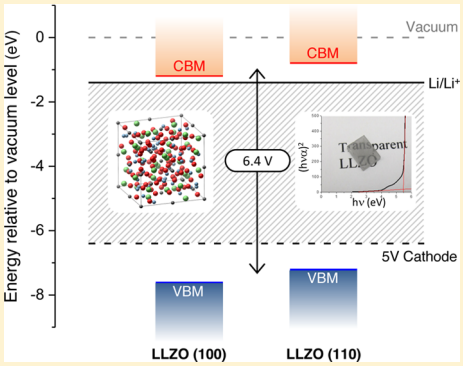

Li-ion battery technology has advanced steadily over the past few decades.[1−4] Despite these advancements, emerging applications such as electric vehicles would benefit considerably from step-change improvements to the cost, safety, longevity, and capacity of Li-ion batteries.[5]

Optimization of Li-ion systems has largely focused on improving electrode properties, for example, by raising the voltage of cathodes and increasing the capacity of anodes.[1] A promising, yet less examined alternative strategy is to replace the battery's liquid electrolyte with a fast ion-conducting solid.[6] A viable solid-state electrolyte could unlock several high-capacity battery concepts. Examples include Li−S batteries, metal−air batteries, solid-state batteries employing Li metal anodes, and all-oxide solid-state Li-ion batteries. The substitution of flammable liquid electrolytes with stable solid-state compounds also offers clear safety advantages.[7,8] Finally, the wide electrochemical window of some solids could enable the use of high-voltage cathodes, resulting in additional gains in energy density.

The garnet mineral structure represents a family of complex oxides spanning a broad range of compositions. Of the possible garnet formulations, the cubic phase with composition $Li_7La_3Zr_2O_{12}$ (LLZO) has recently emerged as one of the most promising solid electrolytes.[7−10] Garnets are typically wide band gap oxides that are expected to be stable at high oxidation potentials.[11,12] Earlier studies have also suggested that some formulations of LLZO are stable against Li metal.[13,14]

These features suggest that high-energy LLZO-based cells combining Li metal anodes and ~5 V cathodes may be within reach. Despite this promise, limited understanding of several properties of LLZO presents potential roadblocks to its implementation. One such property is the electrochemical window (EW). The EW determines an electrolyte's resistance to undesirable electronic transport, and by extension controls phenomena such as short-circuiting and self-discharge. Accurate estimates do not yet exist for basic EW-related properties of LLZO such as its band gap and the positions of its band edges. These properties are now routinely examined in the assessment of liquid electrolytes,[15−18] but have not been thoroughly explored for solid electrolytes. Moreover, experimental measurements of the LLZO EW often employ transient techniques such as cyclic voltammetry (CV), which can be insufficient to determine electronic transport properties.[19] Lacking these data, it is unclear whether the promising performance reported for LLZO represents an intrinsic property of the bulk phase or is instead a consequence of

Received: November 10, 2016
Accepted: January 22, 2017
Published: January 23, 2017

DOI: 10.1021/acsenergylett.6b00593
ACS Energy Lett. 2017, 2, 462−468

fortuitous "kinetic stabilization" arising from interfacial reactions with the electrodes.[1,20,21]

The present study aims to close this knowledge gap by assessing the intrinsic EW of LLZO-based solid electrolytes using multiple experimental techniques and first-principles calculations. Direct current (DC) polarization measurements were performed over a range of voltages of relevance for high-voltage cathodes. These measurements confirm that LLZO is both a fast ion conductor and an excellent electronic insulator, as the fraction of the total current attributable to electronic carriers is less than 10^{-4}. These observations are consistent with the large band gap predicted for LLZO, ranging from 5.5 to 6.4 eV, determined using a combination of optical measurements and quasi-particle calculations. The position of the valence band maximum (VBM) in bulk LLZO further supports the observation of limited electronic transport at high (positive) voltages: p-type conduction arising from hole injection into the valence band is hindered by the low energy of the VBM, which is ~6 V more positive than the Li/Li^+ redox potential. In addition, the conduction band minimum in LLZO is predicted to lie slightly above Li/Li^+, suggesting moderate stability against electron injection (n-type conductivity) from the Li anode. These data indicate that a wide EW is an intrinsic property of LLZO, facilitating its use in next-generation batteries.

Cubic LLZO garnet with the nominal composition $Li_{7-x}La_3Zr_{2-x}Ta_xO_{12}$ (x = 0.25, 0.5, 0.75, and 1.5) and $Li_{6.5}Al_{0.25}La_3Zr_2O_{12}$ were synthesized and assembled into Li/LLZO/Au cells. Details of the sample preparation can be found in previous reports[22] and in the Supporting Information. Chronoamperometric and alternating current (AC) electrochemical impedance spectroscopy (EIS) measurements were used to evaluate the EW of LLZO. Chronoamperometric steps between 3 and 8 V vs Li/Li^+ were held for 2 h, after which the steady-state current was recorded. This current is electronic owing to the semiblocking cell configuration.[23] EIS from 7 MHz to 50 mHz using a 50 mV sinusoidal amplitude was performed at the end of each chronoamperometric step while maintaining the applied bias.

The band gap of Al-doped LLZO was determined by measuring the optical absorption of light transmitted through a dense transparent specimen of $Li_{6.17}Al_{0.28}La_3Zr_2O_{12}$ prepared from hot-pressed powder,[24] cut to 1 mm thickness and polished. The absorption coefficient, α, was measured for wavelengths from 190 to 600 nm (UV-1601, Shimadzu, Japan). A Tauc plot of $(\alpha h\nu)^{1/r}$ versus $h\nu$ was used to determine the optical band gap. Here $h\nu$ is the energy of light, while the exponent r relates to the direct (e.g., $r = 1/2$) or indirect nature of the band gap.[25]

First-principles calculations were used to predict the density of states (DOS), band gap, and absolute positions of the band edges for LLZO. All calculations were performed with the projector-augmented wave method, as implemented in the Vienna Ab initio Simulation Package.[26] Three different levels of theory were employed: (i) the semilocal generalized gradient approximation (DFT-GGA) of Perdew, Burke, and Ernzerhof (PBE);[27] (ii) the hybrid functional of Heyd, Scuseria, and Ernzerhof (HSE06);[28,29] and (iii) quasi-particle (QP) calculations based on many-body perturbation theory (G_0W_0 method).[30] These methods were recently used to predict the band gaps of antiperovskite superionic conductors[31] and the EW of liquid electrolytes at electrode interfaces.[18] A 4-formula-unit primitive cell was used for DOS and band gap calculations, in combination with quasi-random Li-site occupations that satisfy the experimental occupancy ratio of symmetry-equivalent sites.[32] Additional details regarding the computational methods are available in the Supporting Information.

Figure 1 illustrates the Tauc plot used to determine the band gap of LLZO. These data suggest that Al-doped LLZO exhibits

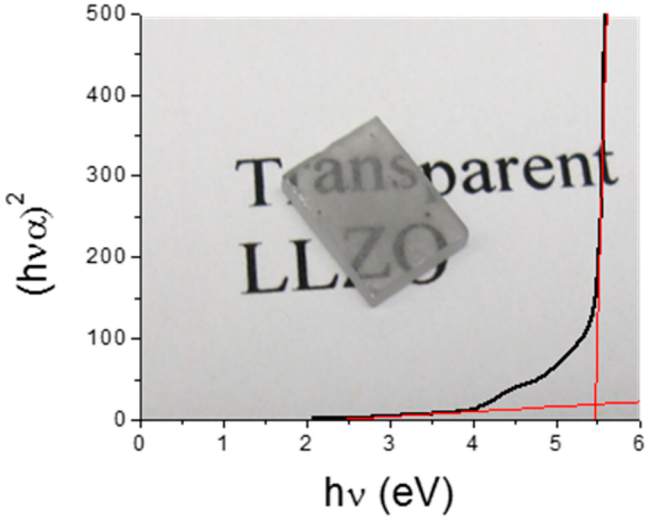

Figure 1. Tauc plot of the optical absorption measurement for Al-doped LLZO, with an optical band gap of 5.46 eV indicated by the intercept of the two fitted lines.

a large optical gap of approximately 5.5 eV. This value agrees well with the band gaps predicted by first-principles computations, shown in Table 1. Band gaps calculated at the HSE06 level of theory are approximately 5.8 eV and are largely insensitive to the Ta or Al doping level. Quasi-particle calculations based on the G_0W_0 method yield slightly larger gaps of 6.07 ($PBE+G_0W_0$) and 6.42 ($HSE06+G_0W_0$) eV (see Figures S1–S3 and Table S1 in the Supporting Information). GW calculations, in particular those based on HSE06 input wave functions, typically yield highly accurate band gaps that are in better agreement with experimental photoemission data than those predicted by hybrid functionals.[33] (The slightly smaller gap suggested by our absorption measurements is likely due to exciton effects, which yield a smaller effective band gap relative to photoemission measurements.) These factors lead us

Table 1. Band Gap, Electronic Conductivity, and Peak Potential for LLZO as a Function of Composition[a]

	0.25 Ta	0.5 Ta	0.75 Ta	1.5 Ta	0.25 Al	undoped LLZO
calculated band gap [eV]	–	5.85	5.83	5.86	5.87	5.79, 6.07,[b] 6.42[c]
measured optical band gap [eV]	–	–	–	–	5.46	
median electronic conductivity [$\times 10^{-9}$ S cm^{-1}]	2.1	1.5	1.4	1.1	1.4	
peak potential [V]	5.0	5.75	5.5	5.5	5.75	
electronic conductivity at min. transference no. [$\times 10^{-9}$ S cm^{-1}]	5.0	2.3	6.2	4.8	5.9	

[a]Unless otherwise indicated, calculated band gaps are reported at the HSE06 level of theory. [b]$PBE+G_0W_0$. [c]$HSE06+G_0W_0$.

DOI: 10.1021/acsenergylett.6b00593
ACS Energy Lett. 2017, 2, 462–468

to conclude that the band gap of LLZO is best approximated by the HSE06+G_0W_0 gap of 6.4 eV.

The large band gap reported here is consistent with earlier CV measurements[34] suggesting that LLZO should be compatible with high-voltage cathodes. Nevertheless, it is important to recognize that a large band gap is a *necessary, but not sufficient* condition for a suitable EW; it is also desirable for the LLZO band edges to be positioned so as to avoid the transfer of electronic species (electrons or holes) to/from the adjacent electrodes. For example, tunneling of electrons into the LLZO conduction band from the negative electrode could generate undesirable n-type electrical conductivity, ultimately short-circuiting the battery. Similarly, the creation of holes in the conduction band via charge transfer to the positive electrode (p-type conductivity) should also be avoided.

The possibility for the emergence of electronic conductivity in LLZO under an applied bias was assessed by measuring the ionic transference number, t_i, as shown in Figure 2a. The

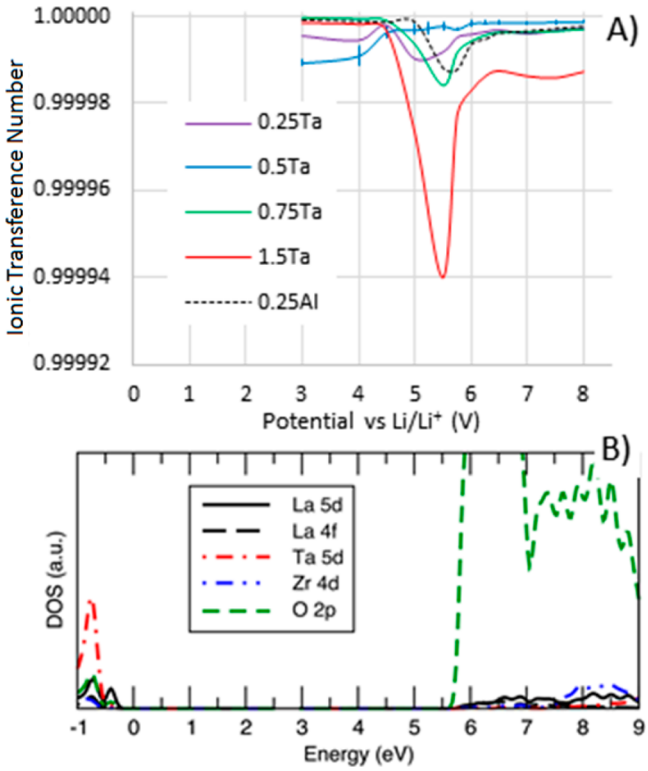

Figure 2. (a) Ionic transference number determined from DC galvanostatic polarization and EIS measurements. (b) Calculated partial density of states for the Ta = 0.75 LLZO composition, illustrating the orbital character of the band edges. The PDOS is scaled to match the band edge positions shown in Figure 3B. The abscissa in both panels is aligned to facilitate comparisons between the transference number and the DOS.

transference number was observed to be nearly equal to 1 (t_i > 0.9999) over the entire voltage window examined and is largely insensitive to the LLZO composition. This indicates that the vast majority (>99.99%) of the conductance arises from ionic transport. Furthermore, because the Li ions migrate within a rigid ceramic framework of ions with far lower mobility (i.e., the Zr, O, and La sublattices), essentially all of the ionic conduction can be attributed to the transport of Li ions. The median electronic conductivity for each composition over the potential range measured is listed in Table 1. These values range from 1.1 to 2.1 × 10^{-9} S/cm and agree well with measurements made at single potential points.[35,36]

While the transference number data indicate that transport in LLZO is almost entirely ionic, we note that the transference number versus voltage data shown in Figure 2A exhibits a small dip near 5.5 V vs Li/Li^+ and then recovers at more positive voltages. Consequently, the 5−6 V region exhibits a slightly higher electronic conductivity; nevertheless, the electronic conductivity never exceeds 0.01% of the ionic conductivity in this voltage window and is an even smaller fraction of the total conductivity outside of this window. As the Ta content decreases from Ta = 1.5 to Ta = 0.5, the magnitude of the dip in t_i also decreases, suggesting a correlation with Ta content. (For Ta = 0.25, the decrease in t_i occurs over a range of voltages. As reported previously,[22] the Ta = 0.25 composition is a mixture of cubic and tetragonal phases, and this most likely accounts for the broader decrease in t_i.) Similar to the Ta = 0.5 composition, the Al-doped LLZO exhibits a dip in t_i near 5.75 V. As described in more detail below, the voltage at which the dip in t_i is observed is similar to the calculated position of the LLZO valence band maximum (VBM). This suggests that the dip in t_i may arise from the injection of holes into the VBM at these voltages.

EIS was performed at each applied bias to confirm that the increase in current associated with the dip in t_i (Figure 2A) arises from an increase in electronic transport. Nyquist plots of the complex impedance data (Figures S4−S10) indicate that the total ionic conductivity does not change with increasing bias. Furthermore, the magnitude of ionic conductivity agrees well with the bulk and total ionic conductivities of Ta-doped samples investigated previously using blocking electrodes.[22,37] As described by Huggins,[23] the low-frequency response of a nonblocking or semiblocking cell can indicate mixed conduction. In the present study, no electronic conduction was observed in the impedance data at open circuit, and the cell exhibited blocking behavior as expected. As the applied bias approached 6 V, the low-frequency response did indeed exhibit an electronic contribution. This contribution decreased again at higher voltages. Thus, the AC data is consistent with the DC data shown in Figure 2A.

Cyclic voltammetry (CV) was performed (Figures S11−S15) on each cell at the conclusion of DC polarization measurements. Similar to previous reports,[34] plating and stripping of Li was observed around 0 V vs Li/Li^+, and no faradaic peaks were observed for applied voltages larger than 3 V vs Li/Li^+. These measurements highlight the inadequacy of the transient CV technique in evaluating the EW: no change in the current flow is observed with CV even though a change in the electronic transport is clearly observed in DC measurements in an equilibrated cell. The combination of DC and AC methods used in the present study allows for the ionic and electronic portions of the total conductivity to be separated. These techniques suggest that the LLZO EW spans the range of voltages tested (up to 8 V), at least for the electrodes used here. Of course, the presence of a realistic cathode, as opposed to the inert Au electrode employed here, could generate interfacial chemical reactions absent from the present cell.[21,38] We next describe why only limited electronic conduction is observed in LLZO, given that the band gap (~6 eV) is smaller than the largest bias tested (8 V).

Density functional theory (DFT) calculations were performed to clarify the electronic conduction mechanism in LLZO. The calculated partial density of states of Ta-doped

DOI: 10.1021/acsenergylett.6b00593
ACS Energy Lett. 2017, 2, 462−468

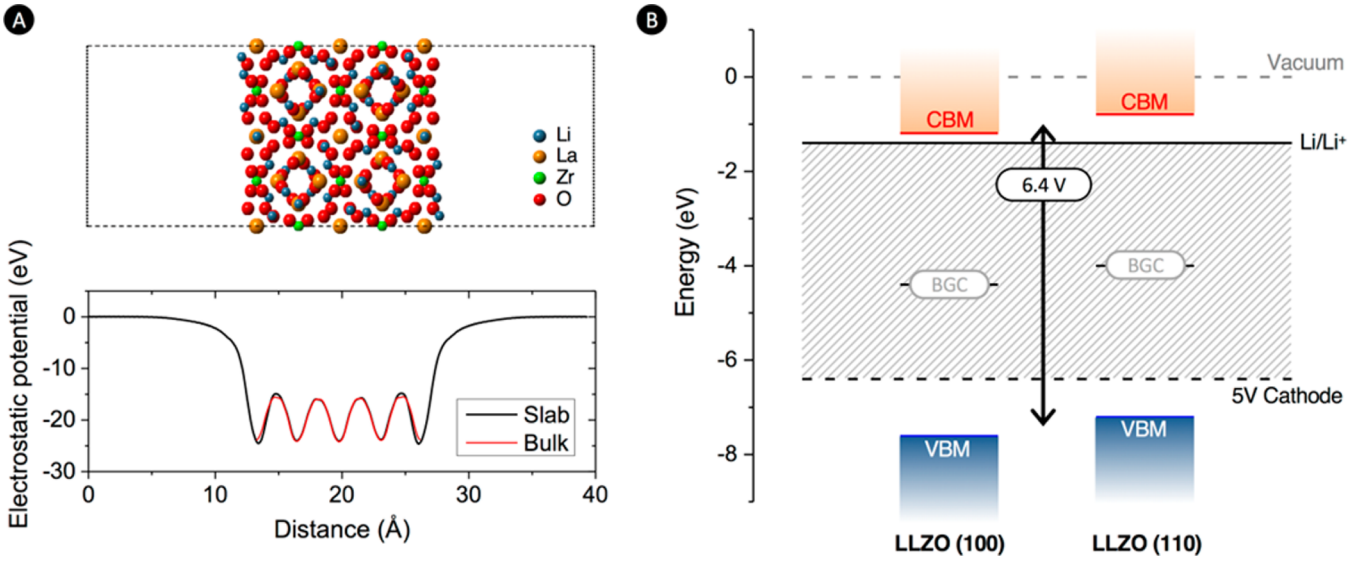

Figure 3. (A) Model of the lowest-energy (100) slab of LLZO (top) and the associated planar-averaged electrostatic potential (bottom panel, black curve). The electrostatic potential from a bulk supercell is overlaid (red data). The vacuum level in the slab supercell corresponds to an electrostatic potential of zero. (B) Position of the conduction band minimum (CBM) and valence band maximum (VBM) of LLZO for the lowest-energy (100) and (110) surface slabs relative to the Li/Li$^+$ level and a hypothetical 5 V cathode. The position of the vacuum level is identified with a dotted gray line, while the band gap center appears as a solid black line.

LLZO is shown in Figure 2B. To facilitate comparisons with the voltage ranges shown in the transference number plot (Figure 2A), the energy axis is mirrored from a standard DOS, such that the conduction bands are plotted at low energy (equivalent to more negative voltages) and the valence bands are shown at higher energy (equivalent to more positive voltages). In addition, the band edge positions are set to match those from our GW calculations, shown in Figure 3B.

With this alignment it is evident that the valence band edge in the DOS coincides with the dip in ionic transference number (Figure 2A and Table 1) near 5.5 V. At these high positive biases, holes are expected to be injected into the valence band, which consists almost entirely of oxygen 2p orbitals. As previously described, the dip in t_i is small in magnitude; similarly, the measured electronic conductivity remains low at all voltages. This behavior can be explained by the localized nature of the orbitals that host the injected holes. Our DFT calculations show that the radius of the O 2p orbitals (as determined by the outermost peak of the radial probability distribution of the free ions) is 0.84 Å. In LLZO, the oxygen−oxygen distance as measured by neutron diffraction is approximately 3 Å,[37] resulting in insignificant overlap of orbitals, which is expected to suppress charge hopping between oxygen sites. Thus, even though biasing the cell to >6 V should induce p-type conductivity, the limited overlap between orbitals (i.e., low mobility of charge carriers) suppresses significant electrical conductivity. Furthermore, the decrease in t_i (Figure 2A) exists for only a narrow voltage window of 5−6 V and disappears for more positive voltages. This behavior seems counterintuitive, because the thermodynamic driving force for hole injection into LLZO should grow as the bias becomes more positive. The measured behavior could be explained, however, by the formation of an electronically insulating interfacial phase (formed by LLZO oxidation products) that blocks further hole injection.

As a general rule, it is desirable for the EW of the electrolyte to exceed the battery's open-circuit voltage (OCV). The OCV is defined as the difference between the electrochemical potentials of the electrodes, η_+ and η_- (i.e., OCV = $\eta_+ - \eta_-$). Similarly, the intrinsic EW of the electrolyte is the difference between its oxidation and reduction levels. In a liquid electrolyte these levels correspond to the highest occupied molecular orbital (HOMO) and lowest unoccupied molecular orbital (LUMO), respectively.

The present study is concerned with a solid-state electrolyte; in this case, the electronic bands of the solid replace the discrete energy levels present in a liquid. Similarly, the solid's band gap (BG) establishes the magnitude of the EW, while the valence band maximum (VBM) and conduction band minimum (CBM) of the solid can be associated with the HOMO and LUMO of the liquid electrolyte, respectively (i.e., VBM ≈ HOMO and CBM ≈ LUMO). Based on these definitions, the criterion for a suitable EW for a solid electrolyte can be recast as BG > OCV. A solid electrolyte that satisfies this requirement will be stable against hole injection (i.e., electrochemical oxidation) from the positive electrode and against electron injection (i.e., electrochemical reduction) from the negative electrode.

The preceding discussion suggests that LLZO has a sufficiently large band gap (6.4 eV) to enable its use with high-voltage electrodes, in principle allowing for an all-solid-state cell with OCV > 6 V. However, it is important to recognize that a large band gap represents a *necessary, but not sufficient condition* for a viable electrolyte; the positions of the band edges relative to the electrochemical potentials of the electrodes are also critical. More specifically, a solid electrolyte will be stable against electron injection if the CBM lies at a higher energy (i.e., more negative potential) than the Fermi level of the negative electrode: E(CBM) > η_-. Similarly, stability against hole injection from the positive electrode requires that the electrolyte's VBM have a lower energy (i.e., be positioned at a more positive potential) than the redox level of the positive electrode: E(VBM) < η_+.

To assess the resistance of LLZO to charge injection and undesirable electronic transport, the absolute positions of the LLZO band edges were evaluated computationally.[39] The

DOI: 10.1021/acsenergylett.6b00593
ACS Energy Lett. 2017, 2, 462−468

calculations employ the planar-averaged electrostatic potential, ϕ, within, and outside of, an LLZO slab. The potential corrugations in the central region of the slab, ϕ_{bulk}, mimic those in bulk LLZO, while the asymptotic behavior of the potential far from the slab establishes the vacuum level, ϕ_{vac}. Knowledge of ϕ_{vac} allows for positioning of the absolute Li/Li$^+$ level (i.e., Li Fermi level).[40] Similarly, the position of the band gap center (BGC) in bulk LLZO can be determined by overlaying ϕ_{bulk} from a bulk LLZO cell onto ϕ_{bulk} from the surface slab. Finally, the absolute positions of the CBM and VBM in bulk LLZO are given by BGC $\pm \frac{E_{gap}}{2}$, where E_{gap} is the band gap evaluated from the present G_0W_0 calculations.

A total of 12 LLZO surface slabs were examined as candidate systems for evaluation of the electrostatic potential (Figures S16−S18). The slabs were constructed to be compositionally symmetric and exhibit (100) and (110) surface normals. (Compositional symmetry does not fully apply to the Li-sublattice, because these sites are known to be partially occupied in a quasi-random fashion.[32]) Six slabs were examined for each surface orientation. (100) and (110) orientations were selected because these orientations commonly yield the lowest-energy surfaces in BCC crystals. (The Zr sublattice in LLZO is BCC.) The slabs with the lowest-energy surfaces were identified after relaxation of their atomic positions. The most stable surfaces, (100) slab #5 and (110) slab #4, were Li terminated and had nearly identical surface energies of 0.84 and 0.85 J/m^2, respectively. Further details regarding the calculations can be found in Tables S2 and S3.

Figure 3A shows the lowest-energy (100) surface along with an overlay of the planar-averaged electrostatic potentials, ϕ, evaluated from the slab and bulk cells. (An equivalent image for the (110) surface is given in Figure S19.) These data were used to determine the absolute positions of the CBM and VBM in bulk LLZO, shown in Figure 3B, for both the lowest-energy (100) and (110) slabs (see also Table S4). To place the band edges in context, the electrochemical potentials of a Li metal anode, η_-, and a hypothetical 5 V cathode, η_+, are also illustrated.

Figure 3B demonstrates that the calculated band edge positions satisfy the electrochemical stability criteria, E(CBM) > η_- and E(VBM) < η_+, regardless of the slab model used. That is, for the Li/5 V couple considered here, bulk LLZO should be susceptible neither to electron injection from the Li negative electrode, nor to hole injection from the cathode.

While the positions of the band edges suggest a suitably wide EW, a few caveats apply. First, as shown by the (100)-oriented slab, the energy difference between the CBM and the Li/Li$^+$ level can be modest, only 0.2 eV in this case. Second, the present band edge model depicts LLZO as a fictitious "isolated" solid, that is, it omits interfacial effects that will be present in a real electrochemical cell and which can potentially narrow[18] or expand the effective EW.[1,21] (For these reasons the EW evaluated here should be interpreted as an intrinsic property of bulk LLZO.) For example, *chemical* reactions at LLZO/electrode interfaces could yield thin product layers that "kinetically stabilize" LLZO by preventing further redox reactions from occurring.[20,21,41] Similarly, *electrochemical* oxidation or reduction at these interfaces could be self-limiting because of the formation of electrically passivating films. Such processes would be similar to those associated with solid−electrolyte interphase (SEI) formation in conventional Li-ion batteries.[1−4] Accounting for these effects will require modeling the full interface at the GW level of theory.[18] Such a calculation is a challenge because of the large size of the LLZO unit cell and the expense of these calculations.

Prior calculations have suggested a stability window for LLZO that is narrower than that predicted in the present study.[20,21] This difference is expected, given that different phenomena, chemical versus electrochemical, are being probed. The present study is concerned with the intrinsic *electrochemical stability*, which is determined by the positions of the CBM and VBM in the bulk solid electrolyte with respect to the electrochemical potentials in the electrodes. In contrast, refs 20 and 21 examine *chemical stability*. There, the (free) energy change due to chemical mixing/reaction is related to a voltage through the Nernst equation.

While chemical and electrochemical stability are both important, they have different implications for performance. Chemical stability is relevant when mixing between reactants is possible (e.g., at the electrolyte/electrode interface). However, the formation of a thickening product layer can ultimately halt the reaction, suggesting that chemical instabilities may not be harmful in all cases. Electrochemical stability is relevant if there is a driving force[1,18] and a pathway for electronic change transfer to or from the electrolyte. Unwanted electrical conductivity in the electrolyte is a consequence of insufficient electrochemical stability.

To cite an example of the interplay between these processes, we note that chemical mixing at the electrolyte/electrode interface can be precipitated by electrochemical charge transfer. Indeed, this is the mechanism associated with SEI formation[15] in conventional Li-ion batteries, where species in the liquid electrolyte are initially reduced by electron transfer from the anode. A series of self-limiting chemical reactions subsequently complete the formation of the SEI. Finally, electrochemical stability can remain a concern even in the presence of an SEI-like layer: charge transfer to (from) the CBM (VBM) can proceed via tunneling through the interlayer.

In summary, DC, AC, and optical measurements were combined with first-principles calculations to systematically characterize the intrinsic electrochemical window of the promising solid electrolyte LLZO. The EW determines an electrolyte's resistance to undesirable electronic transport and, by extension, controls phenomena such as short-circuiting and self-discharge. The position of the EW also impacts electrochemical oxidation and reduction of LLZO by the electrodes; these faradaic processes are generally the first step in subsequent (chemical) reactions at electrolyte/electrode interfaces.[13,14,20,21,42]

Our measurements reveal that LLZO is both a fast ion conductor and an excellent electronic insulator: the fraction of the total current attributable to electronic carriers was observed to be less than 10^{-4} over a range of voltages of relevance for high-voltage cathodes. These observations are consistent with the large band gap (6.4 eV from GW calculations) predicted for LLZO.

An evaluation of the absolute positions of the band edges lends further support to the observation of limited electronic transport in LLZO. A small decrease in the transference number at 5−6 V vs Li/Li$^+$ was shown to coincide with the position of the VBM. Nevertheless, p-type conduction remains very low overall because of limited carrier mobility and/or the formation of an insulating reaction layer. In addition, the conduction band minimum in LLZO is predicted to lie slightly above Li/Li$^+$, suggesting moderate stability against n-type

DOI: 10.1021/acsenergylett.6b00593
ACS Energy Lett. 2017, 2, 462−468

charge injection from the anode. These data indicate that a wide EW window is an intrinsic property of LLZO, furthering its prospects for use in next-generation batteries.

■ ASSOCIATED CONTENT

Supporting Information

The Supporting Information is available free of charge on the ACS Publications website at DOI: 10.1021/acsenergylett.6b00593.

Larger data set from which the representative results shown in the main text are derived (PDF)

■ AUTHOR INFORMATION

Corresponding Authors

*E-mail: djsiege@umich.edu

*E-mail: jeffsaka@umich.edu.

ORCID

Travis Thompson: 0000-0003-3178-3346

Seungho Yu: 0000-0003-3912-6463

Notes

The authors declare no competing financial interest.

■ ACKNOWLEDGMENTS

This work was supported by the U.S. Department of Energy (DOE) Office of Energy Efficiency and Renewable Energy (EERE) Vehicle Technologies Office (VTO) and Advanced Battery Material Research (BMR) program under Grant No. DE-EE-0006821. L.W and E.K. were supported by the National Science Foundation under Grant No. DMR-1561008. Computational resources were provided by the National Energy Research Scientific Computing Center, which is supported by the Office of Science of the U.S. Department of Energy under Contract No. DE-AC02-05CH11231. J.W. and J.L.A. acknowledge support of the U.S. Army Research Laboratory (ARL). S.Y. acknowledges support from the Kwanjeong Educational Foundation. J.S. acknowledges discussions with Prof. Venkataraman Thangadurai who helped to inspire this study.

■ REFERENCES

(1) Goodenough, J. B.; Kim, Y. Challenges for Rechargeable Li Batteries. *Chem. Mater.* **2010**, *22*, 587−603.

(2) Armand, M.; Tarascon, J. M. Building Better Batteries. *Nature* **2008**, *451*, 652−657.

(3) Huggins, R. A. *Advanced Batteries: Materials Science Aspect*; Springer Science and Business Media: New York, 2009.

(4) Bruce, P. G.; Freunberger, S. A.; Hardwick, L. J.; Tarascon, J.-M. Li-O_2 and Li-S Batteries with High Energy Storage. *Nat. Mater.* **2012**, *11*, 19−29.

(5) United States Advanced Battery Consortium. Goals for advanced batteries for EVs, Appendix A.

(6) Teng, S.; Tan, J.; Tiwari, A. Recent Developments in Garnet based Solid State Electrolytes for Thin Film Batteries. *Curr. Opin. Solid State Mater. Sci.* **2014**, *18*, 29−38.

(7) Dudney, N. J.; West, W. C.; Nanda, J. *Handbook of Solid-state Batteries and Supercapacitors*; World Scientific: Hackensack, NJ, 2014.

(8) Takada, K. Progress and Prospective of Solid-State Lithium Batteries. *Acta Mater.* **2013**, *61*, 759−770.

(9) Murugan, R.; Thangadurai, V.; Weppner, W. Fast Lithium Ion Conduction in Garnet-Type $Li_7La_3Zr_2O_{12}$. *Angew. Chem., Int. Ed.* **2007**, *46*, 7778−7781.

(10) Tan, J.; Tiwari, A. Synthesis of Cubic Phase $Li_7La_3Zr_2O_{12}$ Electrolyte for Solid-State Lithium-Ion Batteries. *Electrochem. Solid-State Lett.* **2011**, *15*, A37−A39.

(11) Tomiki, T.; Isa, Y.; Kadekawa, Y.; Ganaha, Y.; Toyokawa, N.; Miyazato, T.; Miyazato, M.; Kohatsu, T.; Shimabukuro, H.; Tamashiro, J. Optical Absorption of Single Crystals of $Y_3Al_5O_{12}$ and $Y_3Al_5O12:Nd^{3+}$ in the UV Fundamental Absorption Edge Region. *J. Phys. Soc. Jpn.* **1996**, *65*, 1106−1113.

(12) Xu, Y.-N.; Ching, W. Y. Electronic Structure of Yttrium Aluminum Garnet ($Y_3Al_5O_{12}$). *Phys. Rev. B: Condens. Matter Mater. Phys.* **1999**, *59*, 10530−10535.

(13) Nemori, H.; Matsuda, Y.; Mitsuoka, S.; Matsui, M.; Yamamoto, O.; Takeda, Y.; Imanishi, N. Stability of Garnet-Type Solid Electrolyte $Li_xLa_3A_{2-y}B_yO_{12}$ (A = Nb or Ta, B = Sc or Zr). *Solid State Ionics* **2015**, *282*, 7−12.

(14) Kim, Y.; Yoo, A.; Schmidt, R.; Sharafi, A.; Lee, H.; Wolfenstine, J.; Sakamoto, J. Electrochemical Stability of $Li_{6.5}La_3Zr_{1.5}M_{0.5}O_{12}$ (M = Nb or Ta) against Metallic Lithium. *Front. Energy Res.* **2016**, *4*. DOI: 10.3389/fenrg.2016.00020.

(15) Xu, K. Electrolytes and Interphases in Li-Ion Batteries and Beyond. *Chem. Rev.* **2014**, *114*, 11503−11618.

(16) Cheng, L.; Assary, R. S.; Qu, X.; Jain, A.; Ong, S. P.; Rajput, N. N.; Persson, K.; Curtiss, L. A. Accelerating Electrolyte Discovery for Energy Storage with High-Throughput Screening. *J. Phys. Chem. Lett.* **2015**, *6* (2), 283−291.

(17) Korth, M. Large-scale virtual high-throughput screening for the identification of new battery electrolyte solvents: evaluation of electronic structure theory methods. *Phys. Chem. Chem. Phys.* **2014**, *16* (17), 7919−7926.

(18) Kumar, N.; Siegel, D. J. Interface-Induced Renormalization of Electrolyte Energy Levels in Magnesium Batteries. *J. Phys. Chem. Lett.* **2016**, *7*, 874−881.

(19) Bard, A. J.; Faulkner, L. R. *Electrochemical Methods: Fundamentals and Applications*; Wiley: New York, 2001.

(20) Miara, L. J.; Richards, W. D.; Wang, Y. E.; Ceder, G. First-Principles Studies on Cation Dopants and Electrolyte|Cathode Interphases for Lithium Garnets. *Chem. Mater.* **2015**, *27*, 4040−4047.

(21) Zhu, Y.; He, X.; Mo, Y. Origin of Outstanding Stability in the Lithium Solid Electrolyte Materials: Insights from Thermodynamic Analyses Based on First-Principles Calculations. *ACS Appl. Mater. Interfaces* **2015**, *7*, 23685−23693.

(22) Thompson, T.; Wolfenstine, J.; Allen, J. L.; Johannes, M.; Huq, A.; David, I. N.; Sakamoto, J. Tetragonal vs. Cubic Phase Stability in Al-Free Ta Doped $Li_7La_3Zr_2O_{12}$ (LLZO). *J. Mater. Chem. A* **2014**, *2*, 13431−13436.

(23) Huggins, R. A. Simple Method to Determine Electronic and Ionic Components of the Conductivity in Mixed Conductors a Review. *Ionics* **2002**, *8*, 300−313.

(24) Yu, S.; Schmidt, R. D.; Garcia-Mendez, R.; Herbert, E.; Dudney, N. J.; Wolfenstine, J. B.; Sakamoto, J.; Siegel, D. J. Elastic Properties of the Solid Electrolyte $Li_7La_3Zr_2O_{12}$ (LLZO). *Chem. Mater.* **2016**, *28*, 197−206.

(25) Davis, E. A.; Mott, N. F. Conduction in Non-Crystalline Systems V. Conductivity, Optical Absorption and Photoconductivity in Amorphous Semiconductors. *Philos. Mag.* **1970**, *22*, 0903−0922.

(26) Kresse, G.; Furthmüller, J. Efficient Iterative Schemes for *ab initio* Total-Energy Calculations Using a Plane-Wave Basis Set. *Phys. Rev. B: Condens. Matter Mater. Phys.* **1996**, *54*, 11169−11186.

(27) Perdew, J. P.; Burke, K.; Ernzerhof, M. Generalized Gradient Approximation Made Simple. *Phys. Rev. Lett.* **1996**, *77*, 3865−3868.

(28) Heyd, J.; Scuseria, G. E.; Ernzerhof, M. Hybrid Functionals Based on a Screened Coulomb Potential. *J. Chem. Phys.* **2003**, *118*, 8207−8215.

(29) Krukau, A. V.; Vydrov, O. A.; Izmaylov, A. F.; Scuseria, G. E. Influence of the Exchange Screening Parameter on the Performance of Screened Hybrid Functionals. *J. Chem. Phys.* **2006**, *125*, 224106.

(30) Shishkin, M.; Kresse, G. Implementation and Performance of the Frequency-Dependent GW Method within the PAW Framework. *Phys. Rev. B: Condens. Matter Mater. Phys.* **2006**, *74*, 035101.

(31) Emly, A.; Kioupakis, E.; Van der Ven, A. Phase Stability and Transport Mechanisms in Antiperovskite Li_3OCl and Li_3OBr Superionic Conductors. *Chem. Mater.* **2013**, *25*, 4663−4670.

(32) Xie, H.; Alonso, J. A.; Li, Y.; Fernández-Díaz, M. T.; Goodenough, J. B. Lithium Distribution in Aluminum-Free Cubic $Li_7La_3Zr_2O_{12}$. *Chem. Mater.* **2011**, *23*, 3587−3589.
(33) Fuchs, F.; Furthmüller, J.; Bechstedt, F.; Shishkin, M.; Kresse, G. Quasiparticle Band Structure Based on a Generalized Kohn-Sham Scheme. *Phys. Rev. B: Condens. Matter Mater. Phys.* **2007**, *76*, 115109.
(34) Ohta, S.; Kobayashi, T.; Asaoka, T. High Lithium Ionic Conductivity in the Garnet-Type Oxide $Li_{7-X}La_3(Zr_{2-X}, Nb_X)O_{12}$ (X = 0−2). *J. Power Sources* **2011**, *196*, 3342−3345.
(35) Rangasamy, E.; Wolfenstine, J.; Sakamoto, J. The Role of Al and Li Concentration on the Formation of Cubic Garnet Solid Electrolyte of Nominal Composition $Li_7La_3Zr_2O_{12}$. *Solid State Ionics* **2012**, *206*, 28−32.
(36) Huang, M.; Liu, T.; Deng, Y.; Geng, H.; Shen, Y.; Lin, Y.; Nan, C.-W. Effect of Sintering Temperature on Structure and Ionic Conductivity of $Li_{7-x}La_3Zr_2O_{12-0.5x}$ (x = 0.5 ∼ 0.7) Ceramics. *Solid State Ionics* **2011**, *204*−*205*, 41−45.
(37) Thompson, T.; Sharafi, A.; Johannes, M. D.; Huq, A.; Allen, J. L.; Wolfenstine, J.; Sakamoto, J. A Tale of Two Sites: On Defining the Carrier Concentration in Garnet-Based Ionic Conductors for Advanced Li Batteries. *Adv. Energy Mater.* **2015**, *5*, 1500096.
(38) Han, F.; Zhu, Y.; He, X.; Mo, Y.; Wang, C. Electrochemical Stability of $Li_{10}GeP_2S_{12}$ and $Li_7La_3Zr_2O_{12}$ Solid Electrolytes. *Adv. Energy Mater.* **2016**, *6*, 1501590.
(39) Toroker, M. C.; Kanan, D. K.; Alidoust, N.; Isseroff, L. Y.; Liao, P.; Carter, E. A. First Principles Scheme to Evaluate Band Edge Positions in Potential Transition Metal Oxide Photocatalysts and Photoelectrodes. *Phys. Chem. Chem. Phys.* **2011**, *13*, 16644−16654.
(40) Sanders, C. R.-G.; Giles, H. W. *Electrode Potentials*; Oxford University Press Inc.: New York, 1998.
(41) Luntz, A. C.; Voss, J.; Reuter, K. Interfacial Challenges in Solid-State Li Ion Batteries. *J. Phys. Chem. Lett.* **2015**, *6*, 4599−4604.
(42) Sharafi, A.; Meyer, H. M.; Nanda, J.; Wolfenstine, J.; Sakamoto, J. Characterizing the Li−$Li_7La_3Zr_2O_{12}$ Interface Stability and Kinetics as a Function of Temperature and Current Density. *J. Power Sources* **2016**, *302*, 135−139.

DOI: 10.1021/acsenergylett.6b00593
ACS Energy Lett. 2017, 2, 462−468